Identifying Lamé Parameters from Time-dependent Elastic Wave Measurements

Armin Lechleiter[a] and John W. Schlasche[a,b**]

[a] *Zentrum für Technomathematik, University of Bremen, Germany*;
[b] *ISEMP, University of Bremen, Germany*

October 12, 2015

Abstract

In many sectors of today's industry it is of utmost importance to detect defects in elastic structures contained in technical devices to guarantee their failure-free operation. As currently used signal processing techniques have natural limits with respect to accuracy and significance, modern mathematical methods are crucial to improve current algorithms. We consider in this paper a parameter identification approach for isotropic and linear elastic structures described by their Lamé parameters and a material density. This approach can be employed for non-destructive defect detection, location and characterization from time-dependent measurements of one elastic wave. To this end, we show that the operator linking the static parameters with the wave measurements is Fréchet differentiable, which allows to set up Newton-like methods for the nonlinear parameter identification problem. We indicate the performance of a specific inexact Newton-like regularization method by numerical examples for a testing problem of a thin plate from measurements of the normal component of the displacement field on the boundary. As an extension, we further augment this method with a total variation regularization and thereby improve reconstructed parameters that feature edges.

1 Introduction

We consider the reconstruction of the material parameters of a linear and isotropic elastic structure from time-dependent measurements of an elastic wave on the surface of a bounded domain of propagation. More precisely, we assume that (known and time-independent) background parameters contain so-called inclusions, that is, subdomains where background parameters are perturbed, and aim to reconstruct the perturbed parameters. To this end, we exploit the differentiability of the operator that maps material parameters to the time-dependent wave field measurements and set up a regularized Newton-like algorithm for parameter identification.

Our basic model for propagation of elastic waves in a bounded domain $\Omega \subset \mathbb{R}^3$ are the equations of time-dependent elasticity linking the displacement field $u : [0,T] \times \Omega \to \mathbb{R}^3$ with the Cauchy stress tensor $\sigma(u) : [0,T] \times \Omega \to \mathbb{R}^{3\times 3}$ in a fixed time interval $[0,T]$ for some $T > 0$,

$$\varrho\, \ddot{u} - \operatorname{div} \sigma(u) = 0 \qquad \text{in } (0,T) \times \Omega, \tag{1}$$

where the divergence operator div is applied row-wise to $\sigma(u)$. Restricting ourselves to a linear, isotropic model, we introduce the symmetric strain tensor $\varepsilon(u) = (Du + (Du)^\top)/2$, involving the Jacobian Du of u, the scalar divergence operator $\operatorname{div} u$, and the 3×3 unit matrix I_3, to prescribe that

**Corresponding author. Email: schlasche@isemp.de

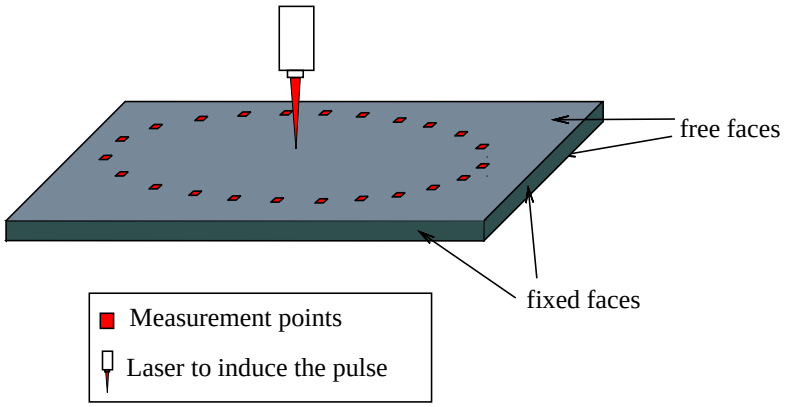

Figure 1: Experimental setup: A laser beam induces a pulse in the plate; components of the generated elastic wave are measured at a couple of positions.

$\sigma(u) = 2\mu\varepsilon(u) + \lambda \operatorname{div} u\, I_3$. Here μ, $\lambda : \Omega \to \mathbb{R}$ denote the Lamé coefficients of the body Ω, linked to the modulus of elasticity E and the Poisson's ratio ν by

$$\mu = E/(2+2\nu) \quad \text{and} \quad \lambda = E\nu/((1+\nu)(1-2\nu)). \tag{2}$$

Thus, (1) can be rewritten as

$$\varrho\, \ddot{u} - 2\operatorname{div}(\mu\varepsilon(u)) - \nabla(\lambda \operatorname{div} u) = 0 \qquad \text{in } (0,T)\times\Omega, \tag{3}$$

This system will be complemented by initial conditions at time $t = 0$ and homogeneous boundary conditions that prescribe that the body is fixed on some non-empty open part $\Gamma \subset \partial\Omega$, i.e., $u = 0$ on $[0,T]\times\Gamma$, while no exterior forces are applied on the remaining boundary $\partial\Omega \setminus \Gamma$. Using the exterior unit normal field n to Ω, this condition reads $\sigma(u)n = 0$ on $\partial\Omega \setminus \Gamma$.

The following experimental setup is one of the many ways in which the approach can be used to identify inhomogeneities in a given part of known geometry. Assume that we generate an elastic ultrasound wave inside Ω by vibrating a (small) part of the boundary $\partial\Omega\setminus\Gamma$ by a piezoelectric actuator or by inducing the wave inside the material using an incident laser beam. The generated ultrasound wave propagates through Ω and its normal component on top of the plate can be recorded in time at a couple of measurement positions by, e.g., optical methods that provide distance information (see Figure 1). Contactless optical measurement techniques avoid the need to build sensors in or on the mechanical structure, which provides an advantage over, e.g., standard strain measurements via piezoelectric sensors or fiber Bragg gratings. The above-introduced parameter identification problem then boils down to the approximation of some of the material parameters μ, λ and ϱ of the plate from such time-dependent wave measurements. (Of course, one could formulate the same identification problem for surface strain measurements instead of field measurements.)

There are various frameworks for establishing existence and uniqueness of solution to the elastic wave equation (3) with suitable boundary conditions and initial values. We rely on the Fourier series-based approach of [1, 2] to obtain (weak) solutions that are continuous in time with values in the Sobolev space H^1 and continuously differentiable in time with values in L^2. As for the scalar wave equation, existence theory can as well be based on a Galerkin or on a semi-group approach, see, e.g., [3], or on the abstract theory on first-order evolution equations in [4]. Under sufficient regularity assumptions on the initial values and the coefficients, higher-order regularity is obtained as in [1,2] for the scalar wave equation. Analogous to the results in [1], we next establish Fréchet differentiability of the solution to the elastic wave equation (3) with respect to its bounded and measurable coefficients;

note that earlier results in the same spirit for the scalar wave equation have been shown in [5]. Let us note here that the existence and differentiability theory for the scalar wave equation in [1, 2] can indeed be applied to any linear second-order wave propagation problem with spatial derivatives that feature a positive-definite bilinear form.

The characterization of the Fréchet derivative and its adjoint via elastic wave equations consequently allows to tackle the identification problem using a successive linearization approach: We opt for the Newton-like regularization method REGINN, see [6, 7], to approximate searched-for parameters numerically. Discretization of the elastic wave equation using finite differences in time and finite elements in space then allows to set up a simulation framework; numerical examples gained within this framework indicate the amount of information that can be gained by this approach. To improve the reconstruction quality for parameters that are piecewise smooth perturbations of the (known) background parameters with jump discontinuities over edges, we couple this Newton-like regularization algorithm with an additional total variation regularization. To this end, we approximate the total variation of a function by a differentiable functional and, after each Newton step, reduce the total variation of the current parameter approximation by a gradient descent step with respect to the smoothed total variation. This enhanced variant of the numerical algorithm improves in particular the reconstruction of edges.

Although we are ultimately interested in numerical algorithms for parameter identification and/or inclusion detection, let us briefly survey uniqueness results for the determination of parameters in wave equations, concentrating on time-dependent and/or elastic problems. Uniqueness results for the parameter $q(t, x)$ of the Schrödinger equation $\ddot{u} - \Delta u + qu = 0$ in $(0, T) \times \Omega$ for given measurements of one wave field on the boundary of a bounded domain go back to [8–11]. Concerning the (static) elastic wave equation, we refer to [12–15] for results on the unique dependence of Lamé coefficients on measurements of (many) Cauchy data of solutions to the time-independent elasticity equation. We further mention the work [16] on the determination of spatially constant elasticity parameters from finitely many measurements of the displacement field. It is however not clear to us whether uniqueness results for the inverse problem considered in this paper do hold; nevertheless, the importance of the problem for applications linked to non-destructive structural testing motivates to develop algorithms that allow at least to approximate some features of the Lamé coefficients.

The structure of the remainder of this paper is as follows: Whilst Section 2 recalls existence analysis for the direct elastic wave propagation problem, Section 3 investigates Fréchet differentiability of the displacement fields with respect to the material parameters. In Section 4, we characterize the L^2-adjoints to these derivatives by solutions to elastic wave equations with particular right-hand sides, and set up an identification algorithm in Section 5. Finally, Section 6 contains details on the implementation of the algorithm and its variant by adding a gradient step with respect to the total variation of the searched-for parameters, together with several numerical examples.

Notation: By $H^s(\Omega)$, $s \in \mathbb{R}$, we denote the usual time-independent Sobolev spaces of scalar functions on a domain $\Omega \subset \mathbb{R}^3$; corresponding Sobolev spaces of vector- or matrix valued functions are denoted by $H^s(\Omega)^3$ or $H^s(\Omega)^{3\times 3}$. The Jacobian matrix of a function $u : \mathbb{R}^3 \mapsto \mathbb{R}^3$ is Du, a matrix in $\mathbb{R}^{3\times 3}$ and $A : B = \sum_{i,j} A_{i,j} B_{i,j}$ denotes the corresponding matrix scalar product. Time and space variables are $t \in \mathbb{R}$ and $x = (x_1, \ldots, x_n)^\top$, respectively; first and second time derivatives are abbreviated by $\dot{u}$ and $\ddot{u}$, respectively. Further, for any Hilbert space V and $T > 0$ the space $C^0([0, T], V)$ contains continuous functions from $[0, T]$ into V, equipped with the maximum norm; analogously, $C^k([0, T], V)$ for $k \in \mathbb{N}$ denotes k-times continuously differentiable functions from $[0, T]$ into V, a normed space when equipped with the sum of the maximum norms of the first k time derivatives and the function itself. The generic constant C might change its value from line to line.

2 Existence, Uniqueness, and Regularity of Solutions to the Elastic Wave Equation

In this section, we adapt a proof for existence and uniqueness to solutions of the scalar wave equation from [1] to the elastic wave equation in a Lipschitz domain $\Omega \subset \mathbb{R}^3$, subject to a spatial excitation $f : [0,T] \times \Omega \to \mathbb{R}^3$ and mixed homogeneous boundary conditions on $\partial\Omega$. On a relatively open and non-empty subset $\Gamma \subset \partial\Omega$ the body is fixed while the complement $\partial\Omega \setminus \overline{\Gamma}$ is free. Thus, the displacement $u : [0,T] \times \Omega \to \mathbb{R}^3$ satisfies

$$\begin{aligned} \varrho\, \ddot{u} - \operatorname{div} \sigma(u) &= f && \text{in } (0,T) \times \Omega, && (4)\\ u &= 0 && \text{on } (0,T) \times \Gamma, && (5)\\ \sigma(u) n &= 0 && \text{on } (0,T) \times \partial\Omega \setminus \overline{\Gamma}, && (6)\\ u(0,\cdot) = u_0,\ \dot{u}(0,\cdot) &= u_1 && \text{in } \Omega, && (7) \end{aligned}$$

and we already introduced the isotropic elastic model $\sigma(u) = 2\mu\varepsilon(u) + \lambda \operatorname{div} u\, I_3$ considered in the following. In the sequel, we are interested in variational (aka weak) solutions to this wave equation, assuming that the material parameters μ, λ and ϱ all belong to $L^\infty(\Omega)$ and satisfy

$$\mu(x) \geq c_\mu > 0, \quad \lambda \geq c_\lambda > 0, \quad \text{and} \quad \varrho \geq c_\varrho > 0 \quad \text{almost everywhere in } \Omega, \tag{8}$$

for arbitrary fixed positive constants c_ϱ, c_μ, and c_λ. We introduce two spaces of real-valued functions,

$$H := L^2(\Omega)^3 \quad \text{and} \quad V := H^1_\Gamma(\Omega)^3 := \left\{ v \in H^1(\Omega)^3 : \, v|_\Gamma = 0 \right\},$$

and assume that the volume force f belongs to $L^2([0,T],H)$ while the initial values u_0 and u_1 belong to V and H, respectively. Note that we abbreviate the L^2-norm and scalar product on H by $\|\cdot\|_H$ and $(\cdot,\cdot)_H$, respectively, and analogously write $\|\cdot\|_V$ and $(\cdot,\cdot)_V$ for the H^1-norm of functions that vanish on Γ.

For the variational formulation of (4-7) we further introduce the Banach space

$$X := C^0([0,T],V) \cap C^1([0,T],H) \quad \text{with norm } \|u\|_X = \left(\max_{0\leq t\leq T} \|u\|_V^2 + \max_{0\leq t\leq T} \|\dot{u}\|_H^2 \right)^{1/2}$$

and its subspace $X_0 = \{v \in X,\, v(0,\cdot) = v(T,\cdot) = 0\}$. Thus, if $u \in X$ (or in X_0), then $\dot{u}(t,\cdot)$ and $\ddot{u}(t,\cdot)$ are well-defined functions in V and in $L^2(\Omega)$ for all $t \in [0,H]$, respectively. Formally multiplying (4) by a test function $v \in X_0$, integrating over $[0,T] \times \Omega$, and integrating by parts in space using the divergence theorem (see [17]), as well as in time, yields that

$$\begin{aligned} \int_0^T \int_\Omega f v \,\mathrm{d}x \,\mathrm{d}t &= \int_0^T \int_\Omega \left[\varrho\, \ddot{u} - 2\operatorname{div}(\mu\varepsilon(u)) - \operatorname{div}(\lambda \operatorname{div} u\, I_3) \right] \cdot v \,\mathrm{d}x \,\mathrm{d}t \\ &= \int_0^T \int_\Omega \left[2\mu\varepsilon(u) : \varepsilon(v) + \lambda \operatorname{div}(u) \cdot \operatorname{div}(v) - \varrho\, \dot{u} \cdot \dot{v} \right] \mathrm{d}x \,, \end{aligned} \tag{9}$$

since $\varepsilon(u)$ is a symmetric matrix. This motivates the definition of the symmetric sesquilinear form

$$a_{\mu,\lambda} : V \times V \to \mathbb{R}, \qquad a_{\mu,\lambda}(u,v) := \int_\Omega \left[2\mu\varepsilon(u) : \varepsilon(v) + \lambda \operatorname{div}(u) \operatorname{div}(v) \right] \mathrm{d}x \,, \tag{10}$$

and to define $u \in X$ to be a variational solution to (4-7) if u satisfies the variational formulation

$$\int_0^T \left[a_{\mu,\lambda}(u,v) - (\varrho\, \dot{u},\, \dot{v})_H \right] \mathrm{d}t \;=\; \int_0^T (f,\, v)_H \,\mathrm{d}t \quad \text{for all } v \in X_0. \tag{11}$$

Since μ and λ are bounded from below away from zero, ellipticity of $a_{\mu,\lambda}$ on V follows from Korn's inequality in $H^1_\Gamma(\Omega)^3$, see, e.g., [17]: There exists $c > 0$ such that

$$\|\varepsilon(u)\|^2_{L^2(\Omega)^{3\times 3}} \geq c\|Du\|^2_{L^2(\Omega)^{3\times 3}} \quad \text{for all } u \in H^1_\Gamma(\Omega)^3. \tag{12}$$

The Dirichlet boundary condition on Γ now implies by Poincaré's inequality that $u \mapsto \|\varepsilon(u)\|_{L^2(\Omega)^{3\times 3}}$ is an equivalent norm on $H^1_\Gamma(\Omega)^3$, such that $a_{\mu,\lambda}$ is indeed elliptic: For some $C > 0$,

$$a_{\mu,\lambda}(u,u) \geq C\|u\|^2_{H^1_\Gamma(\Omega)^3} \qquad \text{for all } u \in H^1_\Gamma(\Omega)^3. \tag{13}$$

Theorem 1. *For all $f \in L^2([0,T],H)$ there exists a unique variational solution $u \in X$ to (11) that is bounded in terms of f, i.e., $\|u\|_X \leq C\|f\|_{L^2([0,T],H)}$.*

Proof. The basic ingredient is a classic energy estimate for solutions to (11) that we briefly sketch here. Assume that $u \in X$ solves (11) with time-derivative $\dot u \in X$ and consider the energy $E(t) := (a_{\mu,\lambda}(u(t),u(t)) + (\varrho\,\dot u(t),\dot u(t))_H)/2$ that is well-defined in $C^1([0,T])$. (Writing $u(t)$, we ignore the spatial argument x here and in what follows.) Differentiating $E(t)$ and integrating by parts in space as in (9) shows that

$$\frac{\partial E}{\partial t}(s) = a_{\mu,\lambda}(u(s),\dot u(s)) + (\varrho\,\ddot u(s),\dot u(s))_H = (f(s),\dot u(s)), \qquad s \in [0,T].$$

After integration in time between between 0 and t we deduce that

$$E(t) \leq E(0) + \int_0^t |f(s)|\,|\dot u(s)|\,\mathrm{d}s \leq E(0) + \sqrt{2}\int_0^t \|\varrho^{-1/2}f(s)\|_H \sqrt{E(s)}\,\mathrm{d}s\,,$$

such that Gronwall's and Jensen's inequality imply that

$$E(t) \leq \left[E(0)^{1/2} + 2^{-1/2}\int_0^t \|\varrho^{-1/2}f(s)\|_H\,\mathrm{d}s\right]^2 \leq 2E(0) + \sqrt{2}\|\varrho^{-1}\|_\infty \int_0^t \|f(s)\|^2_H\,\mathrm{d}s\,.$$

By definition of $E(t)$, this implies the following energy estimate for $t \in [0,T]$,

$$\begin{aligned}\|u(t)\|^2_V + \|\dot u\|^2_H &\leq C\,[a_{\mu,\lambda}(u(t),u(t)) + (\varrho\,\dot u(t),\dot u(t))_H] \\ &\leq C\left[\|u_0\|^2_V + \|u_1\|^2_H + \int_0^t \|f(s)\|^2_H\,\mathrm{d}s\right].\end{aligned}$$

Due to this energy estimate for solutions u such that $\dot u \in V$, existence of solutions to (11) can be shown using, e.g., a Galerkin approach as in [3]; the energy estimate moreover transfers by an approximation argument to solutions $u \in X$ to (11). □

In addition to the latter result, the following regularity theorem for solutions to (11) holds. To this end, we introduce the operator $\Sigma : V \to V'$ from V into its dual V', defined by

$$(\Sigma u, v)_V = a_{\mu,\lambda}(u,v) \qquad \text{for all } u,v \in V. \tag{14}$$

Theorem 2. *If $f \in C^1([0,T],H)$ and if $u_{0,1} \in V$ such that $\Sigma u_0 \in H$ then the solution $u \in X$ to (11) satisfies $u \in C^2([0,T],H) \cap C^1([0,T],V)$ and $\varrho u^{(3)} \in L^2((0,T),V')$ and $\|u\|_X + \|\dot u\|_X \leq C[\|f\|_{C^1([0,T],H)} + \|\Sigma u_0\|_V + \|u_1\|_V]$.*

Since the proof of Lemma 2.4 in [1] can almost literally be copied, we omit the proof.

3 Fréchet Differentiability with Respect to Material Parameters

As we aim to set up a Newton-like algorithm for parameter identification, we compute in this section the Fréchet derivatives of the solution operator to the wave equation (11) with respect to the material parameters, following the approach in [1], where the linearization of the acoustic wave equation with respect to density and wave speed is analyzed. More precisely, if we fix the source term f in (11) and define $\mathcal{D}(L)$ as the set of all triples $(\mu, \lambda, \varrho) \in L^\infty(\Omega)^3$ that satisfy (8), then the main result of this section shows Fréchet differentiability with respect to ϱ, μ, and λ of the solution operator

$$L : \mathcal{D}(L) \subset L^\infty(\Omega)^3 \to X, \qquad (\varrho, \mu, \lambda) \to u \quad \text{where } u \text{ solves (11).} \tag{15}$$

3.1 Auxiliary Results

We start by an auxiliary result on solutions to variational problems with particular right-hand sides that become important when computing Fréchet derivatives later on. As a general assumption we suppose that ϱ, μ, and λ satisfy (8).

Lemma 3. *Assume that $f \in C^1([0,T], H)$, that $u \in X$ solves (11) with initial values $u_0 = 0$ and $u_1 \in V$, and that $h_1, h_2 \in L^\infty(\Omega)$. Then there exist unique solutions $w_1, w_2 \in X$ such that $w_1(0,\cdot) = w_2(0,\cdot) = 0$ and $\dot{w}_1(0,\cdot) = \dot{w}_2(0,\cdot) = 0$ to the variational problems*

$$\int_0^T \left[a_{\mu,\lambda}(w_1, v) - (\varrho\, \dot{w}_1, \dot{v})_H\right] \mathrm{d}t = -\int_0^T a_{h_1,0}(u, v)\, \mathrm{d}t \quad \text{for all } v \in X_0, \tag{16}$$

and

$$\int_0^T \left[a_{\mu,\lambda}(w_2, v) - (\varrho\, \dot{w}_2, \dot{v})_H\right] \mathrm{d}t = -\int_0^T a_{0,h_2}(u, v)\, \mathrm{d}t \quad \text{for all } v \in X_0, \tag{17}$$

that satisfy $\|w_{1,2}\|_X \le C\|h_{1,2}\|_{L^\infty(\Omega)}\|u\|_{C^1([0,T],V)}$. Both w_1 and w_2 also satisfy (16) and (17), respectively, for all $v \in X$ that merely satisfy $v(T) = 0$.

Proof. We follow the proof of Theorem 3.5 in [1] for the scalar wave equation and rewrite the right hand sides of (16) and (17) as scalar products using Riesz's representation theorem: The lower bound (13) gained from Korn's inequality and the Cauchy-Schwarz inequality show that $a_{\mu,\lambda}$ defines a scalar product on V equivalent to the scalar product on $H^1(\Omega)^3$, as $c\|v\|_V^2 \le a_{\mu,\lambda}(v,v) \le C\|v\|_V^2$ for constants $C > c > 0$ and all $v \in V$.

For fixed $u \in X$, both linear forms $v \mapsto a_{h_1,0}(u,v)$ and $v \mapsto a_{0,h_2}(u,v)$ are continuous (for the second form this follows from $|\operatorname{div}(v)|^2 \le |D(v)|^2$), such that for all $t \in [0,T]$ the Riesz representation theorem yields existence of $g_1(t)$ and $g_2(t)$ solving

$$a_{\mu,\lambda}(g_1(t), v) = a_{h_1,0}(u(t), v) \quad \text{and} \quad a_{\mu,\lambda}(g_2(t), v) = a_{0,h_2}(u(t), v) \quad \text{for all } v \in V. \tag{18}$$

Moreover, the assumed regularity of both $f \in C^1([0,T], V)$ and the initial values implies by Theorem 2 that $u \in C^1([0,T], V)$, such that continuity and linearity of the operators mapping $u(t)$ to $g_1(t)$ and $g_2(t)$ implies that $g_{1,2} \in C^1([0,T], V)$, too. By (18), boundedness and coercivity of $a_{\mu,\lambda}$ yields that $\|g_1(t)\|_V \le C\|h_1\|_{L^\infty(\Omega)}\|u(t)\|_V$ as well as $\|\dot{g}_1(t)\|_V \le C\|h_1\|_{L^\infty(\Omega)}\|\dot{u}(t)\|_V$, i.e., $\|g_1\|_{C^1([0,T],V)} \le C\|h_1\|_{L^\infty(\Omega)}\|u\|_{C^1([0,T],V)}$. The same argument shows that $\|g_2\|_{C^1([0,T],V)} \le C\|h_2\|_{L^\infty(\Omega)}\|u\|_{C^1([0,T],V)}$, too. Thus, the lemma's claim follows from the subsequent Lemma 4. □

Lemma 4. *For $g \in C^1([0,T], V)$ the variational problem*

$$\int_0^T \left[a_{\mu,\lambda}(w, v) - (\varrho\, \dot{w}, \dot{v})_H)\right] \mathrm{d}t = \int_0^T a_{\mu,\lambda}(g, v)\, \mathrm{d}t \quad \text{for all } v \in X_0 \tag{19}$$

possesses a unique solution $w \in X$ such that $\|w\|_X \le C\|g\|_{C^1([0,T],V)}$. Further, w satisfies (19) *for all $v \in X$ with $v(T) = 0$.*

If $g \in C_0^2([0,T],V)$ and if $g(0,\cdot) = 0$, then w belongs to $C^2([0,T],H) \cap C^1([0,T],V)$ and $\|w\|_X + \|\dot w\|_X \le C\|g\|_{C^2([0,T],V)}$.

Proof. (1) The spectral theorem for selfadjoint, compact operators and the compact embedding of H in V imply existence of H-orthogonal eigenvectors $\{\varphi_k\} \subset V$ with eigenvalues $\nu_k > 0$ that satisfy $a_{\mu,\lambda}(\varphi_k,\varphi) = \nu_k\,(\varrho\,\varphi_k,\varphi)_H$ for all $\varphi \in V$ and $k \in \mathbb{N}$. By normalizing these eigenvectors with respect to the scalar product $a_{\mu,\lambda}(\cdot,\cdot)$, the $\{\varphi_k\}_{k\in\mathbb{N}}$ moreover are a complete orthonormal system of $(V, a_{\mu,\lambda}(\cdot,\cdot))$; thus, $\{\sqrt{\nu_k}\varphi_k\}_{k\in\mathbb{N}}$ is a complete orthonormal system of $(H, (\varrho\,\cdot,\cdot)_H)$. Due to (8), the latter inner product is equivalent to the standard L^2-inner product $(\,\cdot,\cdot)_H$. Following [1] we search a solution w in series form,

$$w(t,x) = \sum_{k\in\mathbb{N}} w_k(t)\varphi_k(x) \tag{20}$$

and analogously decompose the right-hand side as $g(t,x) = \sum_{k\in\mathbb{N}} g_k(t)\varphi_k(x)$ with time-dependent coefficients g_k given by $g_k(t) = a_{\mu,\lambda}(g(t,\cdot),\varphi_k(t,\cdot))$. (Note that $g_k(0) = 0$.) Depending on the assumed regularity of g, Parseval's equality implies that $\|g\|^2_{C^\ell([0,T],V)} = \sup_{0\le t\le T}\sum_{k\in\mathbb{N}}\sum_{j=0}^{\ell}|g_k^{(j)}(t)|^2$ is finite for $\ell = 0, 1$ or even 2. Due to orthogonality of the φ_k, the scalar coefficients w_k of w need to solve

$$\ddot w_k + \nu_k w_k = \nu_k g_k\,,\ w_k(0) = \dot w_k(0) = 0,$$

compare the proof of Theorem 2.3 in [1]. Thus, $w_k \in C^2([0,T])$ is explicitly given by

$$w_k(t) = \sqrt{\nu_k}\int_0^t \sin(\sqrt{\nu_k}(t-s))g_k(s)\,\mathrm{d}s\,, \qquad t \in [0,T]. \tag{21}$$

Let us now for a moment assume that the series in (20) converges in X and check that, under this condition, w indeed solves (19): Plugging $v(x,t) = \sum_{l=1}^m v_l(t)\varphi_l(x)$ with arbitrary $m \in \mathbb{N}$ and coefficients $v_l \in C^1([0,T])$ such that $v_l(0) = v_l(T) = 0$ into (19), orthogonality of the φ_k yields

$$\begin{aligned}\int_0^T [a_{\mu,\lambda}(w,v) - (\varrho w, v)_H]\,\mathrm{d}t &= \sum_{l,k=1}^m \int_0^T \left(w_k v_l a_{\mu,\lambda}(\varphi_k,\varphi_l) - \dot w_k\dot\varphi_l \frac{(\sqrt{\nu_k}\varphi_k, \sqrt{\nu_l}\varphi_l)_H}{\sqrt{\nu_k}\sqrt{\nu_l}}\right)\mathrm{d}t \\ &= \sum_{k=1}^m \int_0^T \left(w_k v_k - \frac{\dot w_k \dot v_k}{\nu_k}\right)\mathrm{d}t \;= \sum_{k=1}^m \int_0^T v_k\left(w_k + \frac{\ddot w_k}{\nu_k}\right)\mathrm{d}t\,.\end{aligned}$$

As m is arbitrary, a density argument shows that (19) holds.

(2) To show that (19) holds even for $v \in X$ such that merely $v(T) = 0$, choose $\varphi \in V$ and $\psi \in C^1([0,T])$ such that $\psi(0) = \psi(T) = 0$ and plug $v(x,t) = \psi(t)\varphi(x)$ into (19),

$$\int_0^T \Big([a_{\mu,\lambda}(w(t),\varphi) - a_{\mu,\lambda}(g(t),\varphi)]\psi(t) - (\varrho\,\dot w(t),\varphi)_H\dot\psi(t)\Big)\,\mathrm{d}t = 0.$$

As φ and ψ are arbitrary and $t \mapsto a_{\mu,\lambda}(g(t),\varphi)$ is continuously differentiable, we conclude that $t \mapsto (\varrho\,\dot w(t),\varphi)_H$ is continuously differentiable as well and satisfies

$$\frac{\partial}{\partial t}(\varrho\,\dot w(t),\varphi)_H = -a_{\mu,\lambda}(w(t),\varphi) + a_{\mu,\lambda}(g(t,\cdot),\varphi), \qquad t \in [0,T]. \tag{22}$$

Consider now $v \in X$ such that $v(T) = 0$ with representation $v(x,t) = \sum_{k\in\mathbb{N}} v_k(t)\varphi_k(x)$, such that $\varphi_k(T) = 0$ and $\max_{0\le t\le T}\sum_{k\in\mathbb{N}}\left[|v_k(t)|^2 + |\dot v_k(t)|^2/\nu_k\right] \le C\|v\|_X^2$. Plugging in v as a test function into (19) and exploiting orthogonality of the φ_k yields

$$\int_0^T [a_{\mu,\lambda}(w,v) - (\varrho\,\dot w,\dot v)_H)]\,\mathrm{d}t = \sum_{k\in\mathbb{N}}\int_0^T [a_{\mu,\lambda}(w(t),\varphi_k)v_k(t) - (\varrho\,\dot w(t),\varphi_k)_H\,\dot v_k(t)]\,\mathrm{d}t\,,$$

such that integration by parts in time, (22), $v_k(T) = 0$, and $\dot{w}(0) = 0$ imply that

$$\int_0^T \left[a_{\mu,\lambda}(w(t), \varphi_k) + \frac{\partial}{\partial t}(\varrho\, \dot{w}(t), \varphi_k)_H \right] v_k(t)\, \mathrm{d}t \\ - (\varrho\, \dot{w}(T), \varphi_k)_H\, v_k(T) + (\varrho\, \dot{w}(0), \varphi_k)_H\, v_k(0) = \int_0^T a_{\mu,\lambda}(g, \varphi_k) v_k(t)$$

for all $k \in \mathbb{N}$. Thus, (19) holds for all $v \in X$ with $v(T) = 0$.

(3) It remains to prove the regularity of u, i.e., the convergence of the series in (20) in the claimed function spaces. To this end, we exploit estimates for w_k and its derivatives. A partial integration in $[0, T]$ and the initial condition $g_k(0) = 0$ show that

$$w_k(t) = g_k(t) - \int_0^t \cos(\sqrt{\nu_k}(t-s))\dot{g}_k(s)\, \mathrm{d}s \, = \int_0^t [1 - \cos(\sqrt{\nu_k}(t-s))]\dot{g}_k(s)\, \mathrm{d}s$$

for $t \in [0, T]$, such that $|w_k(t)| \leq C\|\dot{g}_k\|_{L^2([0,T])}$. Differentiating (21), integrating by parts again and exploiting that $g_k(0) = 0$ further shows that

$$\begin{aligned} \dot{w}_k(t) &= \nu_k \int_0^t \cos(\sqrt{\nu_k}(t-s)) g_k(s)\, \mathrm{d}s \, = -\sqrt{\nu_k} \int_0^t \sin(\sqrt{\nu_k}(t-s))\dot{g}_k(s)\, \mathrm{d}s \\ &= -\int_0^t \cos(\sqrt{\nu_k}(t-s))\ddot{g}_k(s)\, \mathrm{d}s\,, \qquad t \in [0, T], \end{aligned} \tag{23}$$

such that $|\dot{w}_k(t)| \leq C\|\ddot{g}_k(t)\|_{L^2([0,T])}$. Differentiating (23) with respect to t again shows that $\ddot{w}_k(t) = -\sqrt{\nu_k}\sin(\sqrt{\nu_k}t)\dot{g}_k(0) - \sqrt{\nu_k}\int_0^t \sin(\sqrt{\nu_k}(t-s))\ddot{g}_k(s)\, \mathrm{d}s$ for $t \in [0, T]$, and the continuous embedding of the continuous functions in $H^1([0, T])$ implies that

$$|\ddot{w}_k(t)| \leq \sqrt{\nu_k}\left[|\dot{g}_k(t)| + C\|\ddot{g}_k\|_{L^2([0,T])}\right] \leq C\sqrt{\nu_k}\|g_k\|_{H^2([0,T])}, \quad t \in [0, T]. \tag{24}$$

Let us now first prove that $w \in C^0([0, T], V)$, by showing that the partial sums $w^m(t, x) = \sum_{k=1}^m w_k(t)\varphi_k(x)$ form a Cauchy sequence in $C^0([0, T], V)$. We exploit that the bilinear form $a_{\mu,\lambda}$ defines a scalar product equivalent to the H^1-scalar product: If $m > n$, then

$$\begin{aligned} \max_{0\leq t\leq T} \|w^m(t,\cdot) - w^n(t,\cdot)\|_V^2 &= \max_{0\leq t\leq T} a_{\mu,\lambda}\big(w^m(t,\cdot) - w^n(t,\cdot),\, w^m(t,\cdot) - w^n(t,\cdot)\big) \\ &= \sum_{k=n+1}^m \max_{0\leq t\leq T} |w_k(t)|^2 \leq C \sum_{k=n+1}^m \|\dot{g}_k\|^2_{L^2([0,T])} \leq C\|g\|^2_{C^1([0,T],V)}, \end{aligned}$$

such that the limit w belongs to $C^0([0, T], V)$ if $g \in C^1([0, T], V)$. If, moreover, $g \in C^2([0, T], V)$, the time derivatives of the partial sums w^m are a Cauchy sequence in $C^1([0, T], V)$ as $\|\dot{w}^m(t,\cdot) - \dot{w}^n(t,\cdot)\|_{(V,a_{\mu,\lambda})} \leq C\sum_{k=n+1}^m \|\ddot{g}_k\|^2_{L^2([0,T])} \leq C\|g\|^2_{C^2([0,T],V)}$ for all $t \in [0, T]$. Thus, $w \in C^1([0, T], V)$. Finally, $\ddot{w}$ belongs to $L^2((0, T), H)$, because

$$\|\ddot{w}^m(t,\cdot)\|_H^2 \leq \int_\Omega \varrho|\ddot{w}^m(t,\cdot)|^2\, \mathrm{d}x \, = \sum_{k=1}^m \frac{|\ddot{w}_k(t)|^2}{\nu_k} \leq C\sum_{k=1}^m \|g_k\|^2_{H^2([0,T])} \leq C\|g\|^2_{C^2([0,T],V)}$$

holds for each $t \in [0, T]$. □

3.2 The Fréchet Derivative of the Solution Operator

Next we compute the linearization of parameter-to-state map L introduced in (15) with respect to material parameters μ, λ, and ϱ. We assume again that all these three parameters are essentially bounded and satisfy (8). Recall from (15) that the solution operator maps material parameters to the unique variational solution $u \in X = C^1([0,T],H) \cap C^0([0,T],V)$ to (11), that is,

$$\int_0^T [a_{\mu,\lambda}(u,v) - (\varrho u, v)_H]\,\mathrm{d}t = \int_0^T (f,v)_H\,\mathrm{d}t \quad \text{for all } v \in X_0 = \{z \in X,\ z(0) = z(T) = 0\} \tag{25}$$

with (fixed) initial values $u(0,\cdot) = u_0 \in V$, $\dot{u}(0,\cdot) = u_1 \in H$ and right-hand side $f \in L^2((0,H),H)$.

Theorem 5. *Assume that $u = L(\mu,\lambda,\varrho) \in X$ solves (25) for material parameters $(\mu,\lambda,\varrho) \in \mathcal{D}(L)$, initial data $u_0 = 0$ and $u_1 \in V$, and right-hand side $f \in C^1([0,T],H)$.*

(a) The solution operator L is Fréchet differentiable in (μ,λ,ϱ) with respect to μ and λ. For $h = (h_1,h_2) \in L^\infty(\Omega)^2$, the Fréchet derivative $\nabla_{1,2}L(\mu,\lambda,\varrho) \in \mathcal{L}(L^\infty(\Omega)^2, X)$ with respect to μ and λ is represented by $\nabla_{1,2}L(\mu,\lambda,\varrho)h = w_1 + w_2$, with individual Fréchet derivatives $\partial_{1,2}L(\mu,\lambda,\varrho)h_{1,2} = w'_{1,2} \in X$ with respect to μ and λ that satisfy $w'_{1,2}(0,\cdot) = \dot{w}'_{1,2}(0,\cdot) = 0$ and solve

$$\int_0^T (a_{\mu,\lambda}(w'_1,v) - (\varrho\,\dot{w}'_1,\dot{v})_H)\,\mathrm{d}t = -\int_0^T a_{h_1,0}(u,v)\,\mathrm{d}t \quad \textit{for all } v \in X \textit{ with } v(T) = 0, \tag{26}$$

and

$$\int_0^T (a_{\mu,\lambda}(w'_2,v) - (\varrho\,\dot{w}'_2,\dot{v})_H)\,\mathrm{d}t = -\int_0^T a_{0,h_2}(u,v)\,\mathrm{d}t \quad \textit{for all } v \in X \textit{ with } v(T) = 0. \tag{27}$$

(b) If, additionally, $\Sigma u_1 \in H$ (see (14)) and $f \in C^2([0,T],H)$ with $f(0) = 0$, then L is Fréchet differentiable in (μ,λ,ϱ) with respect to all three parameters μ, λ, and ϱ. For $h = (h_1,h_2,h_3) \in L^\infty(\Omega)^3$, the Fréchet derivative $\nabla L(\mu,\lambda,\varrho) \in \mathcal{L}(L^\infty(\Omega)^3, X)$ is represented by $\nabla L(\mu,\lambda,\varrho)h = w'_1 + w'_2 + w'_3$ with $w'_{1,2}$ from (a) and $w'_3 = \partial_3 L(\mu,\lambda,\varrho)h_3 \in X$ that satisfies $w'_3(0,\cdot) = \dot{w}'_3(0,\cdot) = 0$ and solves

$$\int_0^T (a_{\mu,\lambda}(w'_3,v) - (\varrho\,\dot{w}'_3,\dot{v})_H)\,\mathrm{d}t = \int_0^T (h_3\dot{u},\dot{v})_H\,\mathrm{d}t \quad \textit{for all } v \in X \textit{ with } v(T) = 0. \tag{28}$$

Proof. (a) Our assumptions on u_0, u_1, and $f \in C^1([0,T],H)$ imply by Theorem 2 that u_h and that u belongs to $C^2([0,T],H) \cap C^1([0,T],V)$, such that $\dot{u} \in X = C^1([0,T],H) \cap C^0([0,T],V)$, too. Thus, existence and uniqueness of solution to (26) and (27) follows from Lemma 3. That lemma also provides the bound $\|w'_{1,2}\|_X \le C\|h_{1,2}\|_{L^\infty(\Omega)}\|u\|_{C^1([0,H],V)}$, proving that the linear operators $\partial_1 L(\mu,\lambda,\varrho)$ and $\partial_2 L(\mu,\lambda,\varrho)$ are bounded. We will now show that $w' = w'_1 + w'_2$ is the Fréchet derivative of L with respect μ and λ in direction $h = (h_1,h_2) \in L^\infty(\Omega)^2$. This requires to prove that for $\|h\|_{L^\infty(\Omega)^2}$ small enough it holds that $\|L(\mu+h_1,\lambda+h_2,\varrho) - L(\mu,\lambda,\varrho) - w'_1 - w'_2\|_X \le C\|h\|_{L^\infty(\Omega)^2}$. Setting $u_h = L(\mu+h_1,\lambda+h_2,\varrho)$, where $\|h\|_{L^\infty(\Omega)^2}$ is chosen small enough such that $(\mu+h_1,\lambda+h_2,\varrho) \in \mathcal{D}(L)$, and $d = (u_h - u) - w$ we hence need to estimate $\|d\|_X$. By definition, u_h satisfies $u_h(0) = 0$ and $\dot{u}_h(0) = u_1$ and solves

$$\int_0^T \left[a_{\mu+h_1,\lambda+h_2}(u_h,v) - (\varrho\,\dot{u}_h,\dot{v})_H\right]\mathrm{d}t = \int_0^T (f,v)_H\,\mathrm{d}t \quad \text{for all } v \in X_0,$$

and possesses the same regularity as u. The difference d satisfies $d(0) = 0$, $\dot{d}(0) = 0$, and solves

$$\int_0^T (a_{\mu,\lambda}(d,v) - (\varrho\,\dot{d},\dot{v})_H)\,\mathrm{d}t = \int_0^T a_{h_1,h_2}(u-u_h,v)\,\mathrm{d}t \quad \text{for all } v \in X_0. \tag{29}$$

Thus, Lemma 3 states that $\|d\|_X \le C\|h\|_{L^\infty(\Omega)^2}\|u-u_h\|_{C^1([0,H],V)}$, such that to find an estimate for $\|u_h-u\|_{C^1([0,T],V)}$. Since u_h-u solves

$$\int_0^T (a_{\mu,\lambda}(u_h-u,v)-(\varrho u_h-u,v)_H)\,\mathrm{d}t = -\int_0^T a_{h_1,h_2}(u_h,v)\,\mathrm{d}t \quad \text{for all } v\in C_0^\infty([0,T],V),$$

Lemma 3 states that $\|u_h-u\|_X \le C\|h\|_{L^\infty(\Omega)^2}\|u_h\|_{C^1([0,H],V)} \le C\|h\|_{L^\infty(\Omega)^2}[\|u_1\|_V+\|f\|_{C^1([0,T],H)}]$. We conclude that

$$\|d\|_X \le C\|h\|_{L^\infty(\Omega)^2}\|u-u_h\|_{C^1([0,H],V)} \le C\|h\|^2_{L^\infty(\Omega)^2}\left[\|u_1\|_V+\|f\|_{C^1([0,T],H)}\right].$$

(b) We omit the proof of this part and refer to the proof of Theorem 3.3 in [1]. (The stronger regularity on the initial data and f imply that $h_3\ddot{u}\in L^2([0,T],H)$.) □

We finish this section by a corollary on the Fréchet differentiability of a parameter-to-data operator that maps the volume force f and the initial conditions $u_0=0$ and $v_0=0$ to linear functionals of the solution u to (25).

Corollary 6. *Assume that $f\in C^2([0,T],H)$ with $f(0)=0$ and that $u_0=u_1=0$. If $\Psi: X\to Z$ is a bounded linear operator into a Banach space Z, then $\Psi\circ L:\mathcal{D}(L)\to Z$ is Fréchet differentiable in $(\mu,\lambda,\varrho)\in\mathcal{D}(L)$ with Fréchet derivative*

$$\nabla(\Psi\circ L)(\mu,\lambda,\varrho):\, L^\infty(\Omega)^3\to Z,\quad h\mapsto \Psi\left(\nabla L(\mu,\lambda,\varrho)\right)=\Psi(w_1+w_2+w_3),$$

where the partial derivatives $w_{1,2,3}$ are defined in Theorem 5.

4 The Adjoint of the Fréchet Derivative

Newton-like schemes for parameter identification of material parameters always require to evaluate the adjoint of the Fréchet derivative of the parameter-to-data mapping $\Psi\circ L$. As it is infeasible in our setting to numerically set up the full matrix discretizing this derivative, we characterize this adjoint operator using an elastic wave equation and start by computing the L^2-adjoint of L. Recall that for Hilbert spaces Y and Z and a bounded linear operator $T\in\mathcal{L}(Y,Z)$, the (Hilbert-)adjoint operator is defined by $(y,\,T^*z)_Y=(Ty,\,z)_Z$ for $y\in Y$ and $z\in Z$. As neither $L^\infty(\Omega)$ nor X possess inner products generating equivalent norms, we compute in part (a) of the subsequent theorem a linear operator $(\nabla L(p))^*$ for $p=(\mu,\lambda,\varrho)\in\mathcal{D}(L)$ that is bounded from $L^2([0,T],H)$ into $L^1(\Omega)^3$ and satisfies

$$\big(h,\,(\nabla L(p))^*g\big)_{L^2(\Omega)^3}=(\nabla L(p)h,\,g)_{L^2([0,T],H)} \quad \text{for all } h\in L^\infty(\Omega)^3,\, g\in L^2([0,T],H). \tag{30}$$

Note that we extended the inner product of $L^2(\Omega)$ on the right of the latter equation to a duality product between $L^\infty(\Omega)^3$ and $L^1(\Omega)^3$ and, by abuse of notation, we continue to do so in the sequel.

Theorem 7. *Assume that $f\in C^2([0,T],H)$ with $f(0)=0$ and that $u_0=u_1=0$ and choose $p=(\mu,\lambda,\varrho)\in\mathcal{D}(L)\subset L^\infty(\Omega)^3$.*

(a) For $g\in L^2((0,H),H)$, $(\nabla L(p))^*g=(q_1,q_2,q_3)^\top\in L^1(\Omega)^3$ is represented by $q_{1,2,3}\in L^1(\Omega)$, given by

$$q_1(x)=\int_0^T \varepsilon(u(t,x)):\varepsilon(z(t,x))\,\mathrm{d}t\,,\quad q_2(x)=\int_0^T \operatorname{div}(u(t,x))\cdot\operatorname{div}(z(t,x))\,\mathrm{d}t\,, \tag{31}$$

$$\text{and}\qquad q_3(x)=\int_0^T \dot{u}(t,x)\cdot\dot{z}(t,x)\,\mathrm{d}t\,,\quad \text{a.e. in } \Omega, \tag{32}$$

where $u = L(p) \in X$ solves (25) and $z \in X$ with $z(T) = \dot z(T) = 0$ uniquely solves

$$\int_0^T (a_{\mu,\lambda}(z,v) - (\varrho\,\dot z, \dot v)_H)\,\mathrm{d}t \;=\; \int_0^T (g,v)_H\,\mathrm{d}t \quad \textit{for all } v \in X \textit{ such that } v(0) = 0. \tag{33}$$

(b) There is a bounded and linear operator $(\nabla L(p))^{(*,V)} : L^2((0,T),V) \to L^1(\Omega)^3$ such that

$$\big(h,\, (\nabla L(p))^{(*,V)} g\big)_{L^2(\Omega)^3} = (\nabla L(p)h,\, g)_{L^2([0,T],V)} \quad \left(=: \int_0^T a_{\mu,\lambda}(\nabla L(p)h, g)\,\mathrm{d}t\right) \tag{34}$$

holds for all $h \in L^\infty(\Omega)^3$ and $g \in L^2([0,T],V)$. Again, $(\nabla L(p))^{(*,V)} g = (q_1,q_2,q_3)^\top \in L^1(\Omega)^3$ is given by (31), where $z \in C^2([0,T],H) \cap C^1([0,T],V)$ with $z(T) = \dot z(T) = 0$ uniquely solves

$$\int_0^T (a_{\mu,\lambda}(z,v) - (\varrho\,\dot z, \dot v)_H)\,\mathrm{d}t \;=\; \int_0^T a_{\mu,\lambda}(g,v)\,\mathrm{d}t \quad \textit{for all } v \in X \textit{ such that } v(0) = 0. \tag{35}$$

Remark 8. *(a) At the expense of a more involved proof we could also consider Sobolev spaces with more regularity in time on the right of (34).*

(b) The proof actually shows that $g \mapsto q_3$ is even bounded from $L^2((0,T),H)$ into $L^{6/5}(\Omega)^3$, due to time regularity of u. If one knows a-priori that the spatial regularity of u allows to conclude that $u(t,\cdot) \in L^r(\Omega)^3$ for $r > 2$, then $(\nabla L(p))^*$ also maps into $L^{r/2}(\Omega)^3$; in particular, the Sobolev embedding of $H^1(\Omega)^3$ in $L^6(\Omega)^3$ implies that $(\nabla L(p))^* \in L^3(\Omega)^3$.

Proof. (a) It is clear that determining the adjoint operator $(\nabla L(p))^*$ can be split into three separate problems, since for $h = (h_1,h_2,h_3)$ it holds that

$$(\nabla L(p)h,\, g)_{L^2([0,T],H)} = \sum_{j=1}^3 (\partial_j L(p) h_j, g)_{L^2([0,T],H)} = \big(\sum_{j=1}^3 w_j', g\big)_{L^2([0,T],H)}$$

with $w_{1,2,3}' \in X$ as defined in Theorem 5. Hence we individually compute functions $q_j = q_j(g) \in L^1(\Omega)$ depending on g that satisfy $(h_j, q_j)_{L^2(\Omega)} = (w_j', g)_{L^2([0,T],H)}$, $j = 1,2,3$, such that $(\nabla L(p))^* g = (q_1,q_2,q_3)^\top$. To this end, recall that $u = L(p)\,(= L(\mu,\lambda,\varrho)) \in X$ denotes the solution to (25) that belongs to $C^2([0,T],H) \cap C^1([0,T],V)$ due to our assumptions on u_0, u_1, and $f \in C^2([0,T],H)$ and Theorem 2.

Define $g^{\mathrm{trv}} \in L^2((0,T),H)$ by $g^{\mathrm{trv}}(t) = g(T-t)$ and denote by $z^{\mathrm{trv}} \in X$ the unique solution to

$$\int_0^T (a_{\mu,\lambda}(z^{\mathrm{trv}},v) - (\varrho\,\dot z^{\mathrm{trv}}, \dot v)_H)\,\mathrm{d}t \;=\; \int_0^T (g,v)_H\,\mathrm{d}t \quad \text{for all } v \in X_0, \tag{36}$$

with initial conditions $z^{\mathrm{trv}}(0) = \dot z^{\mathrm{trv}}(0) = 0$; existence and uniqueness of z^{trv} follow from Theorem 1. As in part (2) of the proof of Theorem 19 one shows that the vanishing initial conditions for z^{trv} imply that the latter variational formulation holds even for arbitrary $v \in X$ such that $v(T) = 0$. Thus, the time-reversed function $z \in X$, defined by $z(t) = z^{\mathrm{trv}}(T-t)$, is the unique solution in X of the time-reversed wave equation

$$\int_0^T (a_{\mu,\lambda}(z,v) - (\varrho\,\dot z, \dot v)_H)\,\mathrm{d}t \;=\; \int_0^T (g,v)_H\,\mathrm{d}t \quad \text{for all } v \in X \text{ such that } v(0) = 0, \tag{37}$$

subject to final conditions $z(T) = \dot z(T) = 0$. The stability bound $\|z^{\mathrm{trv}}\|_X \le C\|g\|_{L^2([0,T],H)}$ of Theorem 1 moreover shows that $\|z\|_X \le C\|g\|_{L^2([0,T],H)}$. Because (37) holds for all test functions that vanish at $t = T$, we can in particular choose $v = w_j'$ in (33) and exploit that z itself is also admissible as test function in the variational formulation (26)-(28) of $w_{1,2,3}'$. For simplicity, we treat each case $j = 1,2,3$ individually.

(1) For $j=1$,

$$\int_0^T (g,w_1')_H \,\mathrm{d}t \;=\; \int_0^T (a_{\mu,\lambda}(z,w_1') - (\varrho\,\dot z,\dot w_1')_H)\,\mathrm{d}t \overset{(26)}{=} -\int_0^T a_{h_1,0}(u,z)\,\mathrm{d}t\,.$$

To determine $q_1 = q_1(g) = (\partial_j L(p)h_j)^*$ that satisfies $(g,w_1')_{L^2([0,T],H)} = (h_1,q_1)_{L^2(\Omega)}$ we need to solve

$$-\int_0^T a_{h_1,0}(u,z)\,\mathrm{d}t \;=-\int_0^T\int_\Omega h_1\varepsilon(u):\varepsilon(z)\,\mathrm{d}x\;\mathrm{d}t \overset{!}{=} \int_\Omega q_1(x)\cdot h_1(x)\,\mathrm{d}x\,,$$

and directly conclude that $q_1(x) = \int_0^T \varepsilon(u(t,x)):\varepsilon(z(t,x))\,\mathrm{d}t$. Since

$$\begin{aligned}\|q_1\|_{L^1(\Omega)} &\le \int_\Omega\int_0^T |\varepsilon(u(t))|\,|\varepsilon(z(t))|\,\mathrm{d}t\;\mathrm{d}x \;\le \int_0^T \|\varepsilon(u(t))\|_H\|\varepsilon(z(t))\|_H\,\mathrm{d}t\\ &\le \|u\|_{C^0([0,T],V)}\|z\|_{C^0([0,T],V)} \le \|u\|_{C^0([0,T],V)}\|g\|_{L^2([0,T],H)},\end{aligned}$$

the mapping $g\mapsto q_1$ is bounded from $L^2([0,H],H)$ into $L^1(\Omega)$.

(2) For $j=2$, we find that

$$\int_0^T (g,w_2')_H \,\mathrm{d}t \;=\; \int_0^T (a_{\mu,\lambda}(z,w_2') - (\varrho\,\dot z,\dot w_2')_H)\,\mathrm{d}t \overset{(27)}{=} -\int_0^T a_{0,h_2}(u,z)\,\mathrm{d}t\,.$$

Searching for $q_2 = q_2(g)$ such that $(g,w_2')_{L^2([0,T],H)} = (h_2,q_2)_{L^2(\Omega)}$ leads to

$$\int_0^T a_{0,h_2}(u,z)\,\mathrm{d}t \;=\int_0^T\int_\Omega h_2\cdot\operatorname{div}(u)\cdot\operatorname{div}(z)\,\mathrm{d}x\;\mathrm{d}t \overset{!}{=} \int_\Omega h_2(x)q_2(x)\,\mathrm{d}x\,.$$

Thus, $q_2(x) = \int_0^T \operatorname{div}(u(t,x))\cdot\operatorname{div}(z(t,x))\,\mathrm{d}t$ and $g\mapsto q_2$ is bounded from $L^2([0,H],H)$ into $L^1(\Omega)$, because $\|q_2\|_{L^1(\Omega)} \le \|u\|_{C^0([0,T],V)}\|z\|_{C^0([0,T],V)} \le C\|u\|_{C^0([0,T],V)}\|g\|_{L^2([0,T],H)}$, as for q_1.

(3) For $j=3$, it holds that

$$\int_0^T (g,w_3')_H \,\mathrm{d}t \;=\; \int_0^T (a_{\mu,\lambda}(z,w_3') - (\varrho\,\dot z,\dot w_3')_H)\,\mathrm{d}t \overset{(28)}{=} \int_0^T (h_3\,\dot u,\dot z)_H\,\mathrm{d}t\,,$$

and, as above, we compute that

$$\int_0^T (h_3\,\dot u,\dot z)_H\,\mathrm{d}t \;=\int_\Omega h_3\int_0^T \dot u\cdot\dot z\,\mathrm{d}t\;\mathrm{d}x \overset{(28)}{=} \int_\Omega h_3q_3\,\mathrm{d}x$$

and conclude that $q_3(x) = \int_0^T \dot u(t,x)\cdot\dot z(t,x)\,\mathrm{d}t$. As $\dot u\in C^0([0,T],V)$ and as $V\subset H^1(\Omega)^3$ is continuously embedded in $L^r(\Omega)^3$ for $1\le r\le 6$, we use the generalized Hölder inequality to estimate

$$\begin{aligned}\|q_3\|_{L^{2r/(r+2)}(\Omega)}^{(r+2)/(2r)} &\le \int_\Omega\int_0^T |\dot u\cdot\dot z|^{2r/(r+2)}\,\mathrm{d}t\;\mathrm{d}x \le \int_0^T\int_\Omega |\dot u\cdot\dot z|^{2r/(r+2)}\,\mathrm{d}x\;\mathrm{d}t\\ &= \int_0^T \|\dot u\|_{L^r(\Omega)^3}\|\dot z\|_{L^2(\Omega)^3}\,\mathrm{d}t \le \|u\|_{C^1([0,T],V)}\|z\|_{C^0([0,T],V)} \le \|u\|_{C^1([0,T],V)}\|g\|_{L^2([0,T],H)}.\end{aligned}$$

Thus, $g\mapsto q_3$ is bounded from $L^2([0,T],H)$ into $L^s(\Omega)$ for $1\le s<6/5$ and, in particular, belongs to $\mathcal{L}(L^2([0,T],H),\,L^1(\Omega))$.

Summing up, we have shown that $(\nabla L(p)h)^* = \sum_{j=1}^3 q_j$ satisfies the claimed representation and defines a bounded and linear operator from $L^2((0,T),H)$ into $L^1(\Omega)$.

(b) Replacing the Hilbert space H in the scalar product $(\nabla L(p)h,\,g)_{L^2((0,T),H)}$ on the right of (30) by V in (34) merely requires to change the scalar product $(g,v)_H$ on the right of (36) by $a_{\mu,\lambda}(g,v)$, such that the solution z changes, too. Due to the assumption $f\in C^2([0,T],H)$, Lemma 19 states that the regularity of z thus increases, as both z and $\dot z$ belong to X. Consequently, $g\mapsto q_3$ is even bounded from $L^2((0,T),V)$ into $L^s(\Omega)$ for $1\le s<3$. □

As in the last section, we also consider the adjoint of the Fréchet derivative of the parameter-to-data operator $\Psi \circ L$ from Corollary 6.

Corollary 9. *Assume that $f \in C^2([0,T],H)$ with $f(0) = 0$, that $u_0 = u_1 = 0$, that Z is a Hilbert space, and choose $p = (\mu, \lambda, \varrho) \in \mathcal{D}(L) \subset L^\infty(\Omega)^3$.*

(a) If $\Psi^* : Z \to L^2((0,T),H)$ denotes the adjoint of $\Psi \in \mathcal{L}(L^2([0,T],H),Z)$, then

$$\big(h,\, (\nabla L(p))^* \Psi^* g\big)_{L^2(\Omega)^3} = (\Psi(\nabla L(p)h),\, g)_Z \quad \text{for all } h \in L^\infty(\Omega)^3 \text{ and } g \in Z,$$

where $(\nabla L(p))^* : L^2((0,T),H) \to L^1(\Omega)^3$ has been defined in Theorem 7(a).

(b) If $\Psi^* : Z \to L^2((0,T),V)$ denotes the adjoint of $\Psi \in \mathcal{L}(L^2([0,T],V),Z)$, then

$$\big(h,\, (\nabla L(p))^{*,V} \Psi^* g\big)_{L^2(\Omega)^3} = (\Psi(\nabla L(p)h),\, g)_Z \quad \text{for all } h \in L^\infty(\Omega)^3 \text{ and } g \in Z,$$

where $(\nabla L(p))^{*,V} : L^2((0,T),V) \to L^1(\Omega)^3$ has been defined in Theorem 7(b).

Let us illustrate the last corollary by a crude time-independent model for wave field measurements in time by sensors fixed on $\partial\Omega$: As these sensors cover a certain volume or surface area we choose functions $\{m_i\}_{i=1}^{N_m}$ that either belong to $L^\infty(\Omega)^3$ or to $L^\infty(\partial\Omega)$ and model, e.g., the sensor's coupling to and embedding in the material. Setting

$$(\Psi_\Omega u)_i(t) = \int_\Omega m_i(x) u_j(x,t)\,\mathrm{d}x \quad \text{or} \quad (\Psi_{\partial\Omega} u)_i(t) = \int_{\partial\Omega} m_i(x)\; u|_{\partial\Omega}\,(x,t) \cdot \nu(x)\,\mathrm{d}S \tag{38}$$

for $i = 1, \ldots, N_m$ and some $j \in \{1,2,3\}$ then defines measurement models $\Psi_\Omega : L^2(\Omega)^3 \to (L^2((0,T)))^{N_m}$ or $\Psi_{\partial\Omega} : X \to (L^2((0,T)))^{N_m}$ that are both linear. While boundedness is obvious for Ψ_Ω it requires the trace theorem to prove that $\Psi_{\partial\Omega}$ is bounded,

$$\|(\Psi_{\partial\Omega} u)_j\|_{L^2(0,T)} \le \|m_i\|_{L^\infty(\partial\Omega)} \|u|_{\partial\Omega}\|_{L^2((0,T),L^2(\partial\Omega))} \le \|m_i\|_{L^\infty(\partial\Omega)} \|u\|_{L^2((0,T),V)}.$$

5 The REGINN Algorithm Applied to Parameter Identification

We have now prepared all ingredients to rigorously state the identification problem for the material parameters of the elastic domain Ω we are interested in, and to develop an iterative algorithm for its solution. Recall that $L : \mathcal{D}(L) \subset L^\infty(\Omega)^3 \to X$ denotes the parameter-to-solution operator and that $\Psi : X \to Z$ models a measurement operator mapping the elastic wave $u \in X$ to N_m sensor measurements $\Psi(u)$. (Examples for such measurement operators have been considered in the end of the last section.) Let us further assume that $f \in C^2([0,T],H)$ satisfies $f(0) = 0$, that both initial conditions $u_0 = u_1 = 0$ vanish and that Z is a Hilbert space, such that Corollary 9 implies that the non-linear parameter-to-data operator $\Psi \circ L$ is Fréchet differentiable.

Approximation of the Lamé parameters μ and λ and the material density ϱ from (perturbed) measurements $v_{\text{meas}} \in Z$ of the normal component of one elastic wave at several sensor positions then means to find a solution $p = (\varrho, \mu, \lambda)$ such that

$$\Psi(L(p)) = v_{\text{meas}} \qquad \text{is satisfied for } p = (\varrho, \mu, \lambda) \in \mathcal{D}(L). \tag{39}$$

As uniqueness of this inverse problem is unclear, we are further interested in finding a minimum-norm solution to that problem, that is, a solution with smallest $L^\infty(\Omega)^3$-norm, see [18,19].

As Corollary 9 explicitly characterizes the Fréchet derivative and its adjoint via elastic wave equations, we aim to use a Newton-like scheme for parameter approximation and opt for the so-called REGINN algorithm (REGularization of INverse problems by inexact Newton iterations), see [6,7,20]. This regularization algorithm for non-linear ill-posed problems in Hilbert spaces iteratively linearizes

the non-linear operator equation (39) and computes the jth iteration step h_j from the linearized auxiliary problem

$$\nabla\Psi(L(p_j))h_j = v_{\text{meas}} - \Psi(L(p_{j-1})), \quad j = 1, 2, \ldots, \tag{40}$$

by a truncated conjugate gradient (cg) method in an inner iteration. The step h_j then yields the next iterate $p_{j+1} = p_j + h_j$ for the outer iteration.

Obviously, such a Hilbert space setting does not fit to our above setting with Lamé parameters μ and λ in L^∞. Despite there are Banach space variants of this algorithm, see, e.g., [21], but also [19] for other iterative regularization methods, we rely for simplicity on the Hilbert space version of that algorithm, to avoid implementations of duality mappings. (The variant in [21] requires anyway a reflexive Banach space for the searched-for unknowns which is not the case in our setting.) To this end, we proceed from now on purely formally to obtain a numerical reconstruction algorithm – in other words, we assume that algorithm to be well-posed and indicate its performance by numerical experiments.

The cg-iteration computes iterates $h_{j,i}$ that can be expressed by polynomials $p_{j,i}$ of degree $i \in \mathbb{N}$, depending on the non-linear residual $v_{\text{meas}} - \Psi(L(p_{j-1}))$, such that this method is nonlinear, see [6,22]; setting $F(p_j) = \Psi(L(p_j))$ and $F'(p_j) = \nabla(\Psi \circ L(p_j))$,

$$h_{j,i} = p_{j,i}\big(F'(p_j)^* F'(p_j)\big) F'(p_j)^* [v_{\text{meas}} - F(p_j)], \quad i = 1, 2, \ldots$$

Orthogonality of the cg-polynomials implies that these iterates can be computed by two evaluations of $F'(p_j)$ and $F'(p_j)^*$ using the cg-algorithm, see, e.g., [7, 22] The REGINN algorithm stops the cg-iteration if the linear residual $\|F(p_j) + F'(p_j)h_j - v_{\text{meas}}\|_Z$ is smaller than some tolerance $\theta \in (0, 1)$ times the non-linear residual $\|v_{\text{meas}} - F(p_j)\|_Z$, making the algorithm an inexact Newton method. Finally, the outer iteration in $j \in \mathbb{N}$ is stopped if the discrepancy principle is satisfied, that is, if the nonlinear residual $\|v_{\text{meas}} - F(p_j)\|_Z$ is smaller than the assumed noise level of the data times a constant $\tau > 1$, see [23]. Note that all adjoints in these equations are taken with respect to L^2-inner product (see Theorem 7(a)).

Local convergence of this algorithm to a minimum-norm solution to (39) can be shown under non-linearity conditions on the non-linear operator $\Psi \circ L$ which are usually difficult to verify; whether or not such conditions are satisfied is unclear for many inverse problems in parameter identification (see [7, 20] and [18, 19] for more details). Listing 1 details the REGINN algorithm in pseudo-code.

Listing 1: The REGINN algorithm with inner cg iteration for data v_{meas}, initial guess p_0, noise level ε and parameters $\tau > 1$ for the discrepancy principle and $\theta \in (0, 1)$ for the termination of the inner cg iteration.

```
1  j = 0;
2  //Outer Newton iteration
3  while ‖Ψ(L(p_j)) − v_meas‖_Z > τε‖f‖_{L²([0,T],H)}
4  {
5     i = 0;
6     F(p_j) = Ψ ∘ L(p_j);  F'(p_j) = ∇(Ψ ∘ L(p_j));
7     h_{j,0} = 0;
8     // inner cg iteration
9     while ‖F(p_j) + F'(p_j)h_j − v_meas‖_Z ≥ θ‖F(p_j) − v_meas‖_Z
10    {
11       i = i + 1;
12       // compute ith cg−iterate h_{j,i} by cg−algorithm
13       h_{j,i} = p_{j,i}(F'(p_j)* F'(p_j)) F'(p_j)* [v_meas − F(p_j)];
14    }
15    p_{j+1}=p_j + h_{j,i};
16    j = j + 1;
17 }
```

Tackling (40) with the cg method implies that the adjoint $(\nabla\Psi(L(p_{j-1})))^* = (\nabla L(p))^*\Psi^*$ of the Fréchet derivative is a crucial ingredient of the algorithm; computing $(\nabla L(p))^*\Psi^* g$ for $g \in Z$ via Corollary 9 makes the entire algorithm feasible since this avoids the need to set up the matrix representation of the entire gradient. Section 6 details an implementation of this algorithm using finite elements and presents numerical examples.

6 Implementation and Numerical Examples

As indicated in the introduction, our numerical examples are motivated by non-destructive testing procedures of plates that aim to identify inhomogeneities in a known and homogeneous linearly elastic domain. They shall in particular provide a proof of concept that one can approximate crucial features of spatially varying material parameters from partial measurements of a wave on the boundary of the domain.

To this end, we will actually somewhat simplify the problem and merely attempt to reconstruct a Lamé parameter μ depending on the two variables $x_{1,2}$, defined in a thin plate Ω. For simplicity, we opted to consider a thin quadratic metal plate that is 0.3m long and 0.005m thick. Thus, $\Omega = [0, 0.3] \times [0, 0.3] \times [0, 0.005] \subset \mathbb{R}^3$ and the (background) Lamé parameters equal $\mu_0 = 1.12 \cdot 10^{10}\mathrm{N/m}^2$ and $\lambda_0 = 2.18 \cdot 10^{10}\mathrm{N/m}^2$ (corresponding to the modulus of elasticity $E = 30 \cdot 10^9\mathrm{N/m}^2$ and the Poisson ratio $\nu = 0.33$). Perturbations of these parameters by inclusions will yield parameters to approximate; the density $\varrho = \varrho_0$ of $2.7 \cdot 10^3\mathrm{kg/m}^3$ will always be constant. The top and bottom surface of the plate are traction-free, and the four vertical sides of the plate are fixed, i.e., the displacement field vanishes there; the fixed part $\Gamma \subset \partial\Omega$ introduced in Section 2 hence consists of the four vertical sides of the plate.

For numerical simulations, the domain Ω is discretized by a uniform tetrahedral finite element mesh, consisting of tetrahedra with equilateral triangle base and three equal isosceles triangle sides. The mesh width, i.e., the smallest side of the isosceles triangles, equals 1/700m. This mesh is used to simulate measured data, and to compute Fréchet derivatives in the reconstruction algorithm; A second tetrahedral mesh, the so-called coarse mesh, consists of two layers of mesh points with horizontal mesh width 1/100m. On both meshes, we consider finite element spaces of globally continuous functions that are piecewise linear on the mesh. As we use the coarse mesh to approximate the Lamé parameter μ that is always is a function independent of x_3, the finite element space on the coarse mesh additionally imposes periodic boundary conditions on the top and bottom of the plate.

We simulate the generation of an ultrasound wave inside the plate by inducing a pulse at the center of the plate during a short time interval of approximately 10^{-5}s. More precisely, we model the induced pulse by a volumetric source term $f(t, x) = p(t)s(x)$ for $x \in \Omega$ and $t > 0$. The time-dependent part p of the source is a modulated sine pulse with a central frequency of $4 \cdot 10^5$Hz, given by $p(t) = \sin(4 \cdot 10^5(t - 7 \cdot 10^{-6})) \exp(-0.06(4 \cdot 10^5(t - 8.2 \cdot 10^{-6}))^2)$ if $|t - 8.2 \cdot 10^{-6}| < 4 \cdot 10^{-5}$ and $p(t) = 0$ else. The spatial part s of the pulse equals

$$s(x) = \begin{pmatrix} x_1 - 0.15 \\ x_2 - 0.15 \\ -1 \end{pmatrix} e^{-700((x_1-0.15)^2+(x_2-0.15)^2))},$$

see Figure 2 for the finite element interpolations of these functions on the coarse mesh.

Taking into account technical restrictions for wave measurements, we assume to measure merely the normal component of the elastic wave field $u(t, x_j) \cdot (0, 0, 1)^\top$ at 92 equidistributed points x_j on the boundary of the rectangle $[0.03, 0.27]^2 \times \{0.05\}$ on the top boundary of the plate. This setting yields a crude model for contactless measurements of elastic ultrasound waves induced by a laser beam. Based on these signals we aim to numerically approximate space-dependent material properties of the plate. The discrete version of the measurement operator Ψ thus provides the values of the third component of the displacement field at certain points on the top surface of the plate. (The points x_j are chosen as nodes of the finite element mesh in our experiments.)

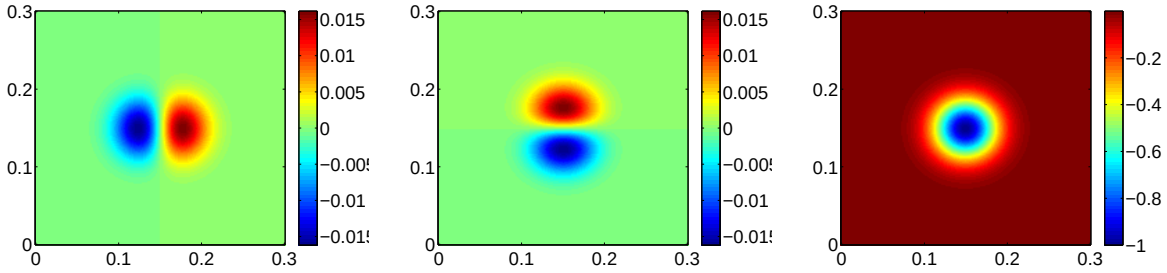

(a) First component of s. (b) Second component of s. (c) Third component of s.

Figure 2: Finite element interpolations of the three components of the spatial part s of the pulse, plotted on the horizontal mid-surface of the plate Ω.

To generate simulated data, we discretize the equations of linear elasticity by the second order central finite difference approximation of the second derivative in time, providing explicit time-stepping up to the inversion of the mass matrix. The bilinear form $a_{\mu,\lambda}$ on $V \times V$ from (10) is discretized by a finite element space of globally continuous functions that are piecewise linear on the mesh of Ω; to this end, we rely on the finite element software FreeFEM++, see [24]. The time-step $\triangle t$ for the simulation of the displacement field is always set to be $\triangle t = 0.5 \cdot \triangle t_{\mathrm{CFL}}$, where $\triangle t_{\mathrm{CFL}}$ is the limiting time step of the Courant–Friedrichs–Lewy condition. The final time $T > 0$ for all simulations of displacement fields, derivatives, and adjoints of derivatives, equals $2.3 \cdot 10^{-4}$s. As we did not attempt to optimize the forward code, an average reconstruction on one core of a workstation with an i7-3770 CPU running at 3.4 GHz took around 110 hours to compute; this could be reduced by, e.g., choosing an optimal time step $\triangle t$ with respect to the mesh width, or by working with cubic meshes.

As was noted before, our numerical experiments consider Lamé parameters that are local perturbations of known constant background parameters $\mu_0 = 1.12 \cdot 10^{10}\mathrm{N/m}^2$ and $\lambda_0 = 2.18 \cdot 10^{10}\mathrm{N/m}^2$ at constant density $\varrho_0 = 2700\mathrm{Kg/m}^3$ and, additionally, do not depend on x_3. As both μ and λ scale linearly with the modulus of elasticity, we further assume that the relative perturbations of μ and λ with respect to the background parameters equal each other, such that $\mu/\mu_0 = \lambda/\lambda_0$. Thus, it suffices to reconstruct μ and to set $\lambda = (\mu/\mu_0)\lambda_0$ (more precisely, in an iterative scheme, the jth iterate μ_j defines λ_j by $(\mu_j/\mu_0)\lambda_0$). This simplification eases the reconstruction task, as merely one Lamé parameter needs to be reconstructed.

It is finally important to note that we compute parameter reconstructions on a coarse mesh with 100 nodes per meter, such that discretizing the formulas from Theorem 7 requires interpolation operators between different finite element spaces. (FreeFem++ provides such interpolation operators as built-in feature.) The interpolation operator $I_{\mathrm{fine}\to\mathrm{coar}}$ from the finite element space on the fine to the finite element space on the coarse mesh is in particular important for the implementation of the adjoint $(\nabla L(p))^*\Psi^*$ in (9): If Ψ_{coar} denotes the discrete measurement operator on the coarse grid and $\nabla L_{\mathrm{fine}}(\mu)$ the Fréchet derivative of the forward operator discretized on the fine grid, the latter adjoint is implemented numerically as $(\nabla L_{\mathrm{fine}}(\mu))^* \circ I^*_{\mathrm{fine}\to\mathrm{coar}} \circ (\Psi_{\mathrm{coar}})^*$.

6.1 Numerical Examples for the REGINN Algorithm

In all our numerical examples shown below, the parameters of the REGINN algorithm in Listing 1 are chosen as $\tau = 1.05$ and $\theta = 0.95$. The chosen value of θ effectively reduces the inner iteration to very few iterations, which turned out to be more time efficient compared to a smaller θ and more inner iterations. For all examples, we add artificial noise to the simulated data. To this end, we scale an array of random numbers that are uniformly distributed in $[-1, 1]$ element-wise such that

the relative noise level equals 25% in the ℓ^2-norm on the data array. The artificial noise level can indeed be chosen that high, since the adjoint of the Fréchet derivative serves as a sort of low pass filter: At a given measurement point, the mean of the added random numbers values is almost zero even for small time intervals, such that solving for the adjoint solution z to (35) filters out most high-frequency noise contained in the right-hand side. The small choice of τ is partly due to the relative small discrepancy resulting from the perturbation of the Lamé parameters when compared with the discrepancy resulting from the artificial noise.

To verify and quantify the reconstruction capabilities of the approach presented in this paper, we test the algorithm using two different perturbation geometries. Results and discussion are summarized in the following two paragraphs. As discussed above, we merely reconstruct the parameter μ, a function depending on (x_1, x_2), and change λ accordingly. In particular, we merely consider μ in the remainder of this section.

Large Inclusion

In this first test we place one large square of side length 0.18m in x_1-direction and 0.042m in x_2-direction near the center of the plate. The contrast for the material parameter μ is constant and equals $-0.5\mu_0$, see Figure 3(a). Figure 3(b) shows that the reconstruction by the REGINN algorithm

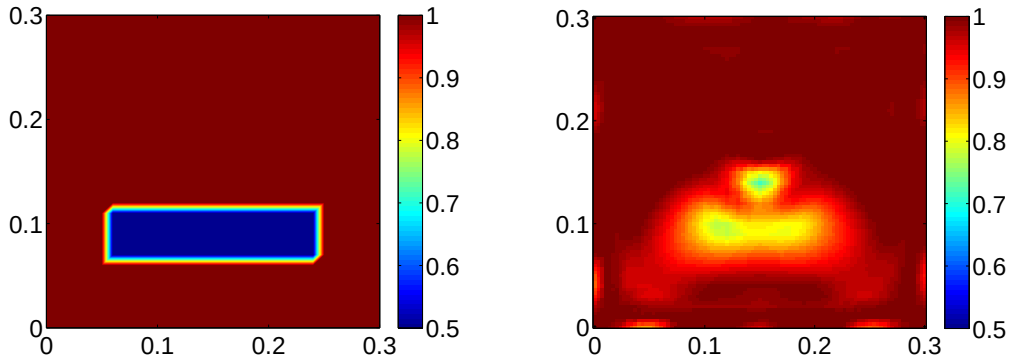

(a) Finite-element interpolation of exact μ/μ_0.

(b) Approximation of μ/μ_0 by the REGINN algorithm.

Figure 3: Approximation of μ/μ_0 with a contrast of $-0.5\mu_0$ by the REGINN algorithm from Listing 1. Plots show the mid-surface of the plate Ω.

from Listing 1 is able to correctly identify the position and geometry of the exact parameter μ. However, the inhomogeneities' edges are smoothed and the contrast does merely reach about half of the correct value. Further, the reconstruction features artifacts close to the plate boundaries, even though the inhomogeneity is placed in the center of the plate. These artifacts may be due to the interpolation error introduced when interpolating functions defined on the fine mesh in the finite element space on the coarse mesh when computing updates of μ and λ as described above. The same comments as apply for the reconstruction shown in Figure 4(b) that has been obtained for the same geometry but a contrast of $0.2\mu_0$.

Multiple Small Inclusions

The second test problem we consider is the approximation of two small inhomogeneities of size 0.042m×0.042m placed close to two opposite corners of the plate. As in the last example, we aim to reconstruct this inhomogeneity for the two contrast values $-0.5\mu_0$ and $0.2\mu_0$. Figure 5(b) shows the

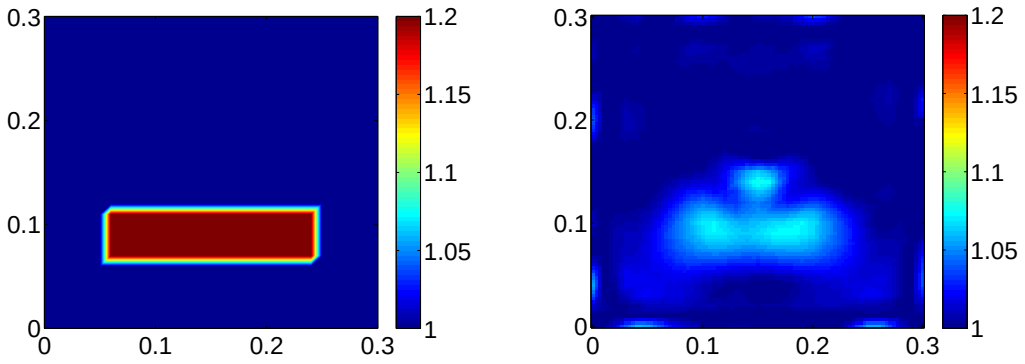

(a) Finite-element interpolation of exact μ/μ_0.

(b) Approximation of μ/μ_0 by the REGINN algorithm.

Figure 4: Approximation of μ/μ_0 with a contrast of $0.2\mu_0$ by the REGINN algorithm from Listing 1. Plots show the mid-surface of the plate Ω.

reconstruction results of the REGINN algorithm from Listing 1 for the negative contrast $-0.5\mu_0$ and Figure 6(b) shows the corresponding results for the contrast $-0.5\mu_0$.

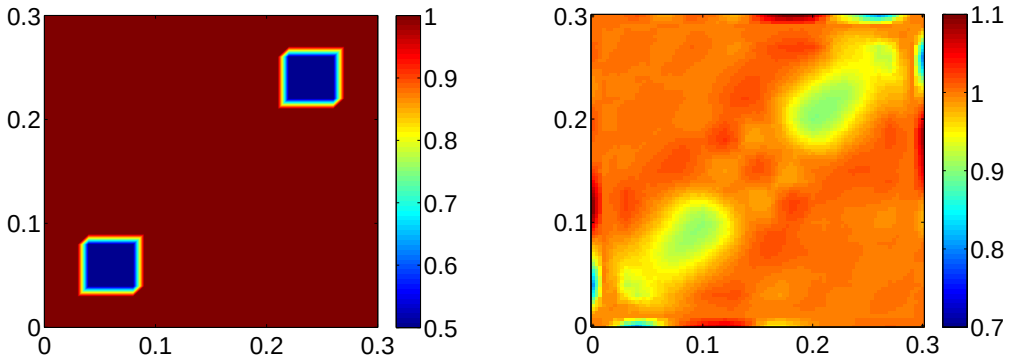

(a) Finite-element interpolation of exact μ/μ_0.

(b) Approximation of μ/μ_0 by the REGINN algorithm.

Figure 5: Approximation of μ/μ_0 with a contrast of $-0.5\mu_0$ by the REGINN algorithm from Listing 1. Plots show the mid-surface of the plate Ω. For better presentation, the colormap has been adjusted in the reconstruction image

In both cases, the parameter reconstructions allow to correctly identify basic features like position or extent of the inclusions, that nevertheless lack even more contrast compared to the examples of Figures 3 and 4. Again, artifacts close to the plate's boundary affect the reconstructions and edges of the inhomogeneities are smoothed, such that their original square shape is completely lost.

6.2 Total Variation-Based Regularization

As we have seen from the reconstructions in Figure 3, the REGINN algorithm fails to reconstruct edges of the Lamé parameter μ from partial measurements of one elastic wave. To promote both the detection of edges and to suppress smoothing effects in the parameter reconstruction, total variation (TV) regularization schemes are often used, particularly in image reconstruction when the aim is,

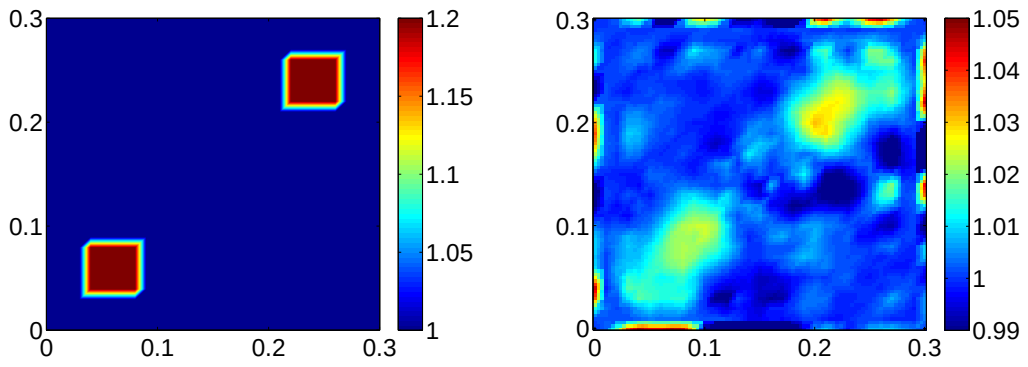

(a) Finite-element interpolation of exact μ/μ_0.

(b) Approximation of μ/μ_0 by the REGINN algorithm.

Figure 6: Approximation of μ/μ_0 with a contrast of $0.2\mu_0$ by the REGINN algorithm from Listing 1. Plots show the mid-surface of the plate Ω. For better presentation, the colormap has been adjusted in the reconstruction image

e.g., to reduce noise by reducing the total variation of an image, see [25]. Variational regularization schemes for the solution of inverse problems often use the total variation of a searched-for parameter by adding this term to a regularizing functional. Our approach here aims to promote the detection of edges of parameters by coupling the gradient descent step of each individual inner iteration step of the REGINN algorithm in Listing 1 with a gradient descent step for the (smoothed) total variation of the parameter. To simplify this approach, we assume that the exact material parameter μ belongs to $H^1(\Omega)$ and approximate the total variation $\mathrm{TV}(\mu) = \int_\Omega |\nabla\mu| \,\mathrm{d}x$ by a smoothed functional with parameter $\beta > 0$,

$$\mathrm{TV}_\beta(\mu) = \int_\Omega \sqrt{\beta^2 + |\nabla\mu|^2} \,\mathrm{d}x\,.$$

A lengthy but straightforward computation shows that the functional TV_β is Fréchet differentiable and that the derivative of that functional at μ in direction $h \in H^1(\Omega)$ equals

$$\nabla\mathrm{TV}_\beta(\mu)h = \int_\Omega \frac{\nabla\mu \cdot \nabla h}{\sqrt{\beta^2 + |\nabla\mu|^2}} \,\mathrm{d}x\,.$$

Thus, the (negative) gradient of the functional at μ equals $\mathrm{div}(\sqrt{\beta^2 + |\nabla\mu|^2}\nabla\mu)$, which is merely an element in the dual of $H_0^1(\Omega)$. Discretizing this expression for small $\beta > 0$ yields a gradient descent direction for the total variation of the searched-for parameter. Alternating this gradient descent step in this direction with the (first) inner iteration of the REGINN algorithm (see Listing 1) then yields a alternating gradient descent method with respect to the squared discrepancy $\|\Psi(L(\mu)) - v_{\mathrm{meas}}\|^2$ and the total variation of μ. This gradient method is purely heuristic and we do not attempt to support it by any theoretic statement.

We further aim to suppress the undesired artifacts close to the boundary that showed up in Figures 3(b)–6(b) by fixing the values of the parameter approximation at the four vertical boundaries of the plate to μ_0 during the iterative reconstruction procedure.

For all computational examples presented below, the parameter β for the TV regularization is set to one and the step width for the gradient descent scheme is set to $8 \cdot 10^4$ for the inclusions from Figures 3(a) and 4(a), and to $8 \cdot 10^3$ for those of Figures 5(a) and 6(a) (These choices are found by trial and error.)

Figure 4 shows that the resulting reconstructions of the four material parameters introduced above show significantly improved edges that are roughly correctly located at the boundaries of the

inclusions, at least for the boundaries closest to the plate's boundary. As the reconstruction appears generally smoother, and in particular almost completely flat outside the inhomogeneity, these reconstructions approximate the exact parameter shapes more accurately than those in Figures 3(b)–6(b). The approximation quality of the reconstructed contrasts depends on the simulated perturbation: In Figure 7(a) and (b) the exact contrasts are better matched compared to the reconstructions shown in Figures 3(a) and 4(a), respectively, while in Figures 7(c) and (d) the contrasts got slightly worse compared to the reconstructions in Figures 6(a) and 6(a), respectively.

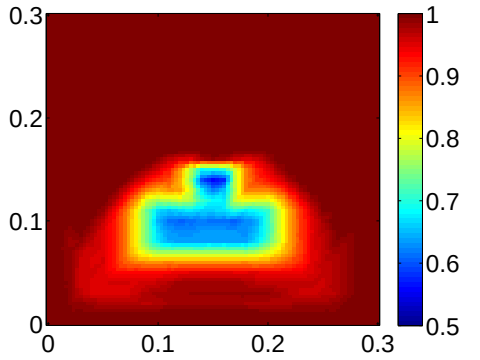

(a) Approximation of μ/μ_0 from Figure 3(a) by the gradient descent scheme with fixed boundary values.

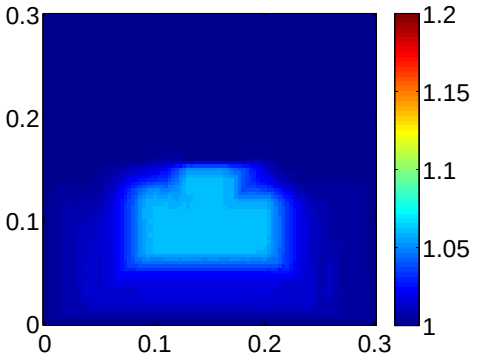

(b) Approximation of μ/μ_0 from Figure 4(a) by the gradient descent scheme with fixed boundary values.

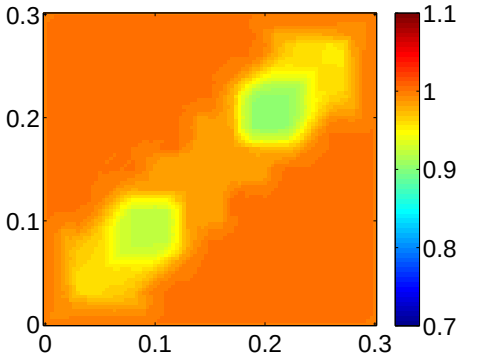

(c) Approximation of μ/μ_0 from Figure 5(a) by the gradient descent scheme with fixed boundary values.

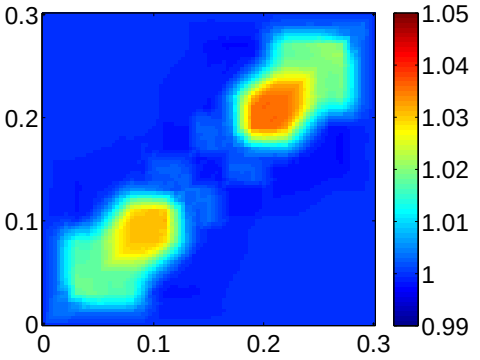

(d) Approximation of μ/μ_0 from Figure 6(a) by the gradient descent scheme with fixed boundary values.

Figure 7: Reconstructions of μ/μ_0 using the alternating gradient descent scheme with respect to the squared discrepancy and the total variation norm of μ. Boundary values of μ/μ_0 are fixed to one during the iterative reconstruction scheme. Plots show the mid-surface of the plate Ω.

7 Conclusion

Based on finite element implementations of solution operator for the elastic wave propagation problem and its Fréchet derivative with respect to the Lamé parameters, we showed that the Newton-like reconstruction algorithm REGINN is able to identify perturbations of constant elastic background parameters, in particular when it is coupled with a smoothed total variation gradient descent. Of course, similar algorithms can be set up for variants of the measurement and/or excitation setup.

As the reconstruction quality of the Lamé parameters depend considerably on the position of the measurement points, the identification of optimal measurement positions might improve the presented results. Further extensions of the presented work are the reconstruction of anisotropic, non-linear or time-dependent elastic material parameters; in particular the last two classes of materials require different approaches, both analytically and algorithmically.

References

[1] Kirsch A, Rieder A. On the linearization of operators related to the full waveform inversion in seismology. Math Meth Appl Sci. 2014;37:2995–3007.

[2] Kirsch A, Hettlich F. The mathematical theory of time-harmonic Maxwell's equations. Applied mathematical series (vol. 190); Heidelberg: Springer; 2015.

[3] Evans L. Partial differential equations. American Mathematical Society; 1998.

[4] Blazek KD, Stolk C, Symes WW. A mathematical framework for inverse wave problems in heterogeneous media. Inverse Problems. 2013;29(6):065001; Available from: `http://stacks.iop.org/0266-5611/29/i=6/a=065001`.

[5] Bao G, Symes WW. On the sensitivity of solutions of hyperbolic equations to the coefficients. Communications in Partial Differential Equations. 1996;21:395–422; Available from: `http://dx.doi.org/10.1080/03605309608821190`.

[6] Rieder A. On the regularization of nonlinear ill-posed problems via inexact Newton iterations. Inverse Problems. 1999;15:309–327.

[7] Rieder A. Inexact Newton regularization using conjugate gradients as inner iteration. SIAM J Numer Anal. 2005;43:604–622.

[8] AL Bukhgeim MK. Global uniqueness of a class of multidimensional inverse problems. Soviet Math Dokl. 1981;24:244–247.

[9] Klibanov MV. Inverse problems and carleman estimates. Inverse Problems. 1992;8:575–596; Available from: `http://dx.doi.org/10.1088/0266-5611/8/4/009`.

[10] Kubo M. Identification of the potential term of the wave equation. Proc Japan Acad Ser A Math Sci. 1995;71:174–176; Available from: `http://dx.doi.org/10.3792/pjaa.71.174`.

[11] Yamamoto M. Uniqueness and stability in multidimensional hyperbolic inverse problems. Journal de Mathématiques Pures et Appliquées. 1999;78:65–98; Available from: `http://dx.doi.org/10.1016/S0021-7824(99)80010-5`.

[12] Nakamura G, Uhlmann G. Global uniqueness for an inverse boundary problem arising in elasticity. Inventiones Mathematicae. 1994;118:457–474; Available from: `http://dx.doi.org/10.1007/BF01231541`.

[13] Nakamura G, Uhlmann G. Erratum: Global uniqueness for an inverse boundary problem arising in elasticity. Inventiones Mathematicae. 2003;152:205–207.

[14] Imanuvilov O, Yamamoto M. On uniqueness of Lamé coefficients from partial cauchy data in three dimensions. J Inv Ill-Posed Prob. 2011;19:881–891.

[15] Imanuvilov O, Uhlmann G, Yamamoto M. On uniqueness of Lamé coefficients from partial cauchy data in three dimensions. Inverse Problems. 2013;28:457–474.

[16] Barbone PE, Gokhale NH. Elastic modulus imaging: on the uniqueness and nonuniqueness of the elastography inverse problem in two dimensions. Inverse Problems. 2004;20:283; Available from: http://stacks.iop.org/0266-5611/20/i=1/a=017.

[17] McLean W. Strongly elliptic systems and boundary integral operators. Cambridge, UK: Cambridge University Press; 2000.

[18] Kaltenbacher B, Neubauer A, Scherzer O. Iterative regularization methods for nonlinear ill-posed problems. Berlin: de Gruyter; 2008.

[19] Schuster T, Kaltenbacher B, Hofmann B, Kazimierski KS. Regularization methods in banach spaces. Berlin: de Gruyter; 2012.

[20] Lechleiter A, Rieder A. Towards a general convergence theory for inexact Newton regularizations. Numer Math. 2010;114:521–548.

[21] Margotti F, Rieder A. An inexact Newton regularization in banach spaces based on the nonstationary iterated tikhonov method. J Inv Ill-posed Probl. 2014;.

[22] Hanke M. Regularizing properties of a truncated Newton-cg algorithm for nonlinear inverse problems. Numer Funct Anal Optim. 1998;18:971–973.

[23] Engl HW, Hanke M, Neubauer A. Regularization of inverse problems. Dordrecht, Netherlands: Kluwer Acad. Publ.; 1996.

[24] Hecht F. New development in FreeFem++. J Numer Math. 2012;20:251–265.

[25] Scherzer O, Grasmair M, Grossauer H, Haltmeier M, Lenzen F. Variational methods in imaging. Vol. 167 of Applied Mathematical Sciences. New York: Springer; 2009.